Inorg. Chem. **2003**, *42*, 5771–5777

Spectroscopic and Structural Characterization of the $[Fe(imidazole)_6]^{2+}$ Cation

Graham Carver,[†] Philip L. W. Tregenna-Piggott,*[,†] Anne-Laure Barra,[‡] Antonia Neels,[§] and John A. Stride[||]

Department of Chemistry, University of Bern, Freiestrasse 3, Bern 9, CH-3000 Switzerland, Grenoble High Magnetic Field Laboratory, 25 avenue des Martyrs, BP166, 38042 Grenoble, Cedex 9, France, Institut de Chimie, Université de Neuchâtel, Avenue de Bellevaux 51, CP 2, CH-2007 Neuchâtel, Switzerland, and Institut Laue-Langevin, BP156, 38042 Grenoble, Cedex 9, France

Received January 31, 2003

Spectroscopic, structural, and magnetic data are presented for $Fe(C_3H_4N_2)_6(NO_3)_2$, which facilitate a precise definition of the electronic and molecular structure of the $[Fe(Im)_6]^{2+}$ cation. The structure was determined at 120(1) K by X-ray diffraction methods. The salt crystallizes in the trigonal space group $R\bar{3}$ with unit-cell parameters $a = 12.4380(14)$ Å, $c = 14.5511(18)$ Å, and $Z = 3$. All the imidazole ligands are equivalent with an Fe–N bond distance of 2.204(1) Å. Variable-temperature inelastic neutron scattering (INS) measurements identify a cold magnetic transition at 19.4(2) cm^{-1} and a hot transition at 75.7(6) cm^{-1}. The data are interpreted using a ligand field Hamiltonian acting in the weak-field ^5D basis, from which the diagonal trigonal field splitting of the $^5T_{2g}$ (O_h) term is estimated as $\sim$485 cm^{-1}, with the ^5A_g (S_6) component lower lying. High-field multifrequency (HFMF) EPR data and measurements of the magnetic susceptibility are also reported and can be satisfactorily modeled using the energies and wave functions derived from analysis of the INS data. The electronic and molecular structures are related through angular overlap model calculations, treating the imidazole ligand as a weak π-donor.

1. Introduction

The imidazole ring, as a histidine moiety, functions as a ligand towards transition metal ions in a number of biologically important molecules. In particular, it is found coordinated to iron in hemoglobin, myoglobin, and cytochrome *c*.[1,2] The majority of previous studies on iron(II)−imidazole complexes have focused on model systems, resembling the naturally occurring low-symmetry environments, which are necessarily so complicated that the role of the individual ligators is difficult to determine.[3,4] Our approach is to study high-symmetry homoleptic complexes, in order to obtain an understanding of the iron−imidazole interaction by the determination of the ground-state electronic structure.

The physical methods most commonly employed to study Fe(II) complexes are Moessbauer spectroscopy[5,6] and the measurement of the magnetic moment,[6] from which the energies of the low-lying states may be inferred. The ground electronic structures of a number of homoleptic Fe(II) complexes have been probed previously with the aid of far-IR spectroscopy[7] and high-field multifrequency (HFMF) EPR.[8,9] A direct spectroscopic determination is also afforded by inelastic neutron scattering (INS), and this technique has been the method of choice for the characterization of a number of integer-spin transition metal complexes.[10,11] In this

* To whom correspondence should be addressed. E-mail: tregenna@iac.unibe.ch.
[†] University of Bern.
[‡] Grenoble High Magnetic Field Laboratory.
[§] Université de Neuchâtel.
[||] Institut Laue-Langevin.

(1) Hughes, M. N. *The Inorganic Chemistry of Biological processes*, 2nd ed.; John Wiley: New York, 1981.
(2) Huheey, J. E. *Inorganic Chemistry-Principles of structure and Reactivity*, 3rd ed.; Harper International: London, 1983.
(3) Louro, R. O.; Correia, I. J.;Brennan, L.; Coutinho, I. B.; Xavier, A. V.; Turner, D. L. *J. Am. Chem. Soc.* **1998**, *120*, 13240.
(4) Soltis, S. M.; Strouse, C. E. *J. Am. Chem. Soc.* **1988**, *110*, 2824.
(5) Little, B. F.; Long, G. J. *Inorg. Chem.* **1978**, *17(12)*, 3401−3413.
(6) Reedijk, J. *Rec. Trav. Chim.* **1971**, *90*, 1285−1291.
(7) Champion, P. M.; Sievers, A. J. *J. Chem. Phys.* **1977**, *66*, 1819−1825.
(8) Knapp, J.; Krzystek, J.; Brunel, L.-C.; Hendrickson, D. N. *Inorg Chem.* **2000**, *39*, 281−288.
(9) Smith, G. M.; Riede, P. C. *Electron Paramagn. Reson.* **2000**, *17*, 164−204.
(10) Dobe, C.; Andres, H. P.; Tregenna-Piggott, P. L. W.; Mossin, S.; Weihe, H.; Janssen, S. *Chem. Phys. Lett.* **2002**, *362*, 387−396.

10.1021/ic034110t CCC: $25.00 © 2003 American Chemical Society
Published on Web 08/14/2003

paper, INS data for $Fe(Im)_6(NO_3)_2$ are presented and modeled using a ligand field Hamiltonian operating in the ^5D basis. Good agreement with experiment is obtained for a narrow range of values of λ and Δ, which represent the spin−orbit coupling constant and the trigonal field splitting of the $^5T_{2g}$ (O_h) ground term, respectively. HFMF EPR and susceptibility data for $Fe(Im)_6(NO_3)_2$ are presented and modeled by extending the Hamiltonian to include the Zeeman interaction. Simulations based on the best-fit ligand field parameters obtained from INS give good agreement with experiment. The solution of the crystal structure facilitates the determination of angular overlap model (AOM) bonding parameters, which can be used to predict the electronic ground structure of other iron(II) complexes containing the imidazole ligand.

2. Experimental Details

Aqueous $Fe(NO_3)_2$ solution (0.9 M, deoxygenated) was prepared by the addition of $FeSO_4 \cdot 7H_2O$ (5 g, 18 mmol) to an aqueous solution of $Pb(NO_3)_2$ (5.96 g, 18 mmol in 20 mL, deoxygenated) and stirring for 10 min. The fine precipitate of $PbSO_4$ was allowed to settle and the pale green supernatant $Fe(NO_3)_2$ solution extracted by means of a syringe. A 10 mL volume of this solution was added to a solution of imidazole (30 mL, 3.2 M, deoxygenated) and the resulting mixture passed through a Schlenk filter. The filtrate was left at ~5 °C under argon to crystallize, yielding approximately 2.1 g of ~0.2 mm colorless $Fe(Im)_6(NO_3)_2$ crystals. The C, H, and N content was determined by elemental analysis. (Anal. Found: C, 37.16; H, 4.11; N, 33.45. Calcd for $FeC_{18}H_{24}N_{14}O_6$: C, 36.75; H, 4.11; N, 33.33.)

Deuterated $Fe(Im)_6(NO_3)_2$ was made in a similar manner using deuterated starting materials. $FeSO_4 \cdot XD_2O$ (~5 g, 18 mmol Fe^{2+}) was made by the recrystallization of 5 g (18 mmol) $FeSO_4 \cdot 7H_2O$ from 3 × 50 mL D_2O under argon, and an $Fe(NO_3)_2$ solution in D_2O was subsequently prepared from $Pb(NO_3)_2$ in D_2O and $FeSO_4 \cdot XD_2O$, as described above. Addition of $Fe(NO_3)_2$ solution (10 mL, 0.9 M, in D_2O, deoxygenated) to a solution of deuterated imidazole (30 mL, 3.2 M, in D_2O, deoxygenated) gave ~4.3 g of a fine white powder of deuterated $Fe(Im)_6(NO_3)_2$ (yield ~ 78%). The latter was characterized by powder X-ray diffraction and shown to be isostructural with the hydrogenous salt.

The X-ray diffraction intensity data of a colorless crystal of hydrogenous $Fe(Im)_6(NO_3)_2$ were collected at 120 K on a Stoe image plate diffraction system[12] using Mo Kα graphite-monochromated radiation, image plate distance 70 mm, ϕ oscillation scans 0−150°, step $\Delta\phi = 1.5°$, 2θ range 4.03−25.86, and $d_{max} - d_{min} = 12.45-0.81$ Å. The structure was solved by direct methods and refined by least-squares techniques in the anisotropic approximation for all non-hydrogen atoms using the programs SHELXS-97[13] and SHELXL-97.[14] All hydrogen atoms were localized in difference Fourier maps and refined isotropically. The crystal was very regular in shape, and both the μ-value (0.64 mm^{-1}) and the maximum e-density (0.237 e $Å^{-3}$) are small; hence, no correction for absorption or extinction was applied.

Inelastic neutron scattering measurements were performed on the instruments IN4, at the Insitut Laue-Langevin in Grenoble, France, and on FOCUS, at the Paul Scherrer Institute in Villigen, Switzerland.

In the INS experiment, neutrons of a known initial kinetic energy E_i are scattered by the sample in the direction specified by the polar angles θ and ϕ into an element of solid angle $d\Omega = \sin(\theta)\, d\theta\, d\phi$. The number of neutrons scattered/s into $d\Omega$ with a final kinetic energy between E_f and $E_f + dE_f$ is given by the partial differential cross section $d^2\sigma/d\Omega\, dE_f$ (where σ is the total number of neutrons scattered in all directions/s). This is the quantity measured in the experiment. During a scattering event the neutron can lose energy to the sample (Stokes process) or gain energy from the sample (anti-Stokes process) thus creating or annihilating an excitation, respectively. Through the interaction, momentum is also transferred to the sample as a function of the scattering direction, and it is possible to extract the neutron cross section as a function of momentum transfer, Q. The dependence of the partial differential cross section, and hence the peak intensities, on the momentum transfer differs for magnetic and phonon transitions, thus providing a means by which these transitions can be distinguished in the INS spectrum.[15,16]

In compounds containing hydrogen, the large incoherent cross section of the proton often precludes the possibility of observing magnetic INS transitions. Consequently measurements were conducted on a ~5 g crystalline powder sample of the deuterated $Fe(Im)_6(NO_3)_2$ salt. The sample was loaded into a thin-walled (~0.5 mm) aluminium cylinder (external diameter 10 mm, length 50 mm) and sealed under a helium atmosphere.

HFMF EPR measurements were performed at the Grenoble High Magnetic Field Laboratory at the CNRS in Grenoble, France; the apparatus has been described in detail previously.[17,18] Powdered samples of the hydrogenous $Fe(Im)_6(NO_3)_2$ salt were examined at temperatures of 5−40 K, employing frequencies of 190−475 GHz. The samples were prepared by grinding crystals of $Fe(Im)_6(NO_3)_2$ under dry nitrogen. The powder was then mixed thoroughly with an equal quantity of *n*-eicosane wax (mp 36 °C, 95%, Fluka) to prevent the crystallites aligning in a strong magnetic field[19] and loaded into a standard 4 mm diameter quartz EPR tube to a depth of about 1.5 cm. The tube was sealed under a helium atmosphere at a height of ca. 10 cm. The wax was melted by immersion of the tube in warm water, and subsequent cooling yielded a ca. 1 cm long solid white pellet.

Magnetic susceptibility measurements of a powdered sample of $Fe(Im)_6(NO_3)_2$ were conducted on a Quantum Design MPMS-XL SQUID magnetometer, at the University of Bern. Crystals of the hydrogenous $Fe(Im)_6(NO_3)_2$ were ground under dry nitrogen, and the sample (19.2 mg) was sealed in a gelatine capsule. Measurements were obtained using a field-strength of 0.1 T at temperatures of 1.8−300 K.

3. Results and Discussion

3.1. Crystal Structure. X-ray diffraction measurements confirm that this compound is isomorphous with the Co^{2+}, Ni^{2+}, and Cd^{2+} salts.[20−22] The space group is $R\bar{3}$ with the

(11) Basler, R.; Tregenna-Piggott, P. L. W.; Andres, H.; Dobe, C.; Gudel, H.; Janssen, S.; McIntyre, G. J. *J. Am. Chem. Soc.* **2001**, *123*, 3377−3378.
(12) *IPDS Software*; Stoe & Cie GmbH: Darmstadt, Germany, 2000.
(13) Sheldrick, G. M. SHELXS-97 Program for Crystal Structure Determination. *Acta Crystallogr.* **1990**, *A46*, 467, 473.
(14) Sheldrick, G. *SHELXL-97*; Universität Göttingen: Göttingen, Germany, 1999.
(15) Gudel, H. U. *Molecular Magnetism: From Molecular Assemblies to the Devices*; Coronado, E., et al., Eds.; Kluwer Academic Publishers NL: Dordrecht, The Netherlands, 1996; pp 229−242.
(16) Squires, G. L. *Introduction to the theory of thermal neutron scattering*; Cambridge University Press: New York, 1979.
(17) Muller, F.; Hopkins, A.; Coron, N.; Ggrynberg, M.; Brunel, L.-C.; Martinez, G. *Rev. Sci. Instrum.* **1989**, *60*, 3681.
(18) Barra, A. L.; Brunel, L.-C.; Robert, J. B. *Chem Phys. Lett.* **1990**, *165*, 107.
(19) Krzystek, J.; Telser, J.; Pardi, L. A.; Goldberg, D. P.; Hoffman, B. M.; Brunel, L.-C. *Inorg. Chem.* **1999**, *38*, 6121.
(20) Mighell, A. D.; Santoro, A. *Acta Crystallogr.* **1971**, *B27*, 2089.

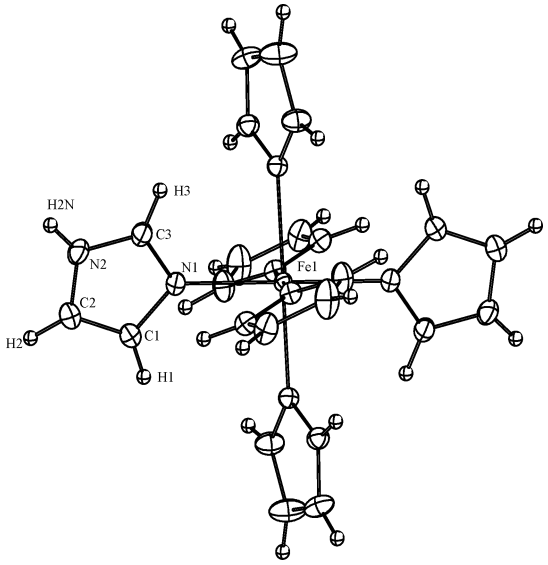

Figure 1. Geometry of the $[Fe(Im)_6]^{2+}$ cation in the $Fe(Im)_6(NO_3)_2$ salt as determined by X-ray diffraction. Displacement ellipsoids are drawn at the 50% probability level.

Table 1. Crystal Data and Structure Refinement for $Fe(C_3H_4N_2)_6(NO_3)_2$

empirical formula	$C_{18}H_{24}FeN_{14}O_6$
cryst color	colorless
fw	588.36
temp	120(2) K
cryst system	trigonal
space group	$R\bar{3}$
unit cell dimens	$a = 12.4380(14)$ Å
	$b = 12.4380(14)$ Å
	$c = 14.5511(18)$ Å
V	1949.5(4) Å^3
Z	3
D(calcd)	1.503 g/cm^3
linear abs coeff	0.643 mm^{-1}
radiatn, wavelength	0.710 73 Å (Mo Kα)
F(000)	912
diffractometer	STOE IPDS
scan method	ϕ oscillation
θ range for data collection	4.03−25.86°
limiting indices	$-15 \le h \le 15$, $-15 \le k \le 15$, $-15 \le l \le 17$
no. of reflcns measd	3720 [R(int) = 0.0649]
indepndt/obsd reflcns	831/777
refinement method	full-matrix least squares on F^2
data/restraints/params	831/0/76
goodness-of-fit on F^2	1.078
final R indices [$I > 2\sigma(I)$]	R1 = 0.0270, wR2 = 0.0695
max Δ/σ	0.005
$(\Delta\rho)_{max}$	0.237 Å^{-3}
$(\Delta\rho)_{min}$	−0.212 Å^{-3}

$[Fe(Im)_6]^{2+}$ complex on a site of S_6 symmetry. The imidazole ligands are all crystallographically equivalent; the plane of the imidazole ring is rotated about the Fe−N bond vector by an angle, φ,[23] of 22° relative to the regular FeN_6 octahedral framework (Figure 1). The crystal data are given in Table 1, and selected bond lengths and angles are listed in Table 2. Fractional coordinates and thermal displacement parameters are included in the Supporting Information. The

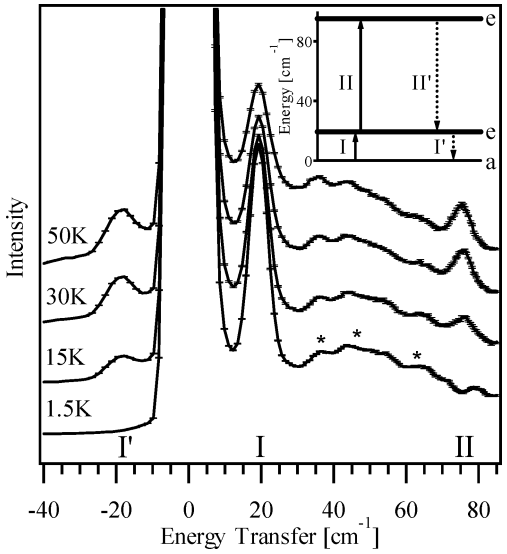

Figure 2. INS spectra of a crystalline powder sample of deuterated $Fe(Im)_6(NO_3)_2$ as a function of temperature. The transitions are denoted in the inset.

Fe−N bond distance is 2.204(1) Å, which is similar to those found in other octahedral high-spin iron(II) compounds containing imidazole derivatives as ligands.[24,25]

3.2. Inelastic Neutron Scattering. INS spectra, recorded on the time-of-flight spectrometer IN4, at temperatures of 1.5, 15, 30, and 50 K are shown in Figure 2.[26] An incident wavelength of 2.2 Å was selected, which afforded the observation of energy transfers up to 120 cm^{-1}, with a resolution of ca. 5 cm^{-1}.

At 1.5 K, the spectrum consists of an intense band at 19.4(2) cm^{-1}, labeled I in Figure 2, and a number of weaker bands at higher energy. Upon increasing the temperature, a band emerges at 75.7(6) cm^{-1} (transition II), identifying this as a hot transition. The intensities of bands I and II were found to decrease with increasing momentum transfer, Q, indicating that they correspond to transitions of magnetic origin.[16] Figure 3 shows plots of the intensity of transition I, as a function of Q, at various temperatures. The experimental points are represented by symbols. The lines depict the expected intensities, calculated using empirical functions and tabulated coefficients for the spin-only magnetic form factor of Fe(II) and weighted with a Boltzmann factor.[27] The intensities of the other much weaker features marked with an asterisk increase sharply with increasing Q, which is a signature of phonon transitions.[16] Both magnetic bands are observed on the neutron energy gain side (designated by

(21) Santoro, A.; Mighell, A. D.; Zocchi, M.; Reimann, C. W. *Acta Crystallogr.* **1969**, *B25*, 842.
(22) Prince, E.; Mighell, A. D.; Reimann, C. W.; Santoro, A. *Cryst. Struct. Commun.* **1972**, *1*, 247−252.
(23) Dolder, S.; Spichiger D.; Tregenna-Piggott, P. L. W. *Inorg. Chem.* **2003**, *42*, 1343−1349.
(24) Garciá-Vázquez, J. A.; Romero, J.; Sousa-Pedrares, A.; Sousa, A.; Garnovskii, A. D.; Garnovskii, D. A. *J. Chem. Cryst.* **2000**, *30*, 23−26.
(25) Seel, F.; Lehnert, R.; Bill, E.; Trautwein, A. *Z. Naturforsch., B: Anorg. Chem., Org. Chem.* **1980**, *35B(5)*, 631−8.
(26) The detectors were calibrated by means of a vanadium metal spectrum. Vanadium scatters isotropically and hence is ideally suited for this purpose. A cylindrical vanadium sample was chosen to mirror the geometry of the sample. A background spectrum of an empty aluminium container was subtracted from the data; the time-of-flight to energy conversion and data reduction were performed with the program LAMP.
(27) *International Tables for Crystallography*; Kluwer Academic Publishers: Dordrecht, The Netherlands, 1995; Vol. C.

Table 2. Selected Bond Lengths (Å) and Angles (deg) for $Fe(C_3H_4N_2)_6(NO_3)_2$

C(1)−C(2)	1.357(2)	C(2)−C(1)−N(1)	109.59(14)
C(1)−N(1)	1.3832(19)	C(1)−C(2)−N(2)	106.05(14)
C(2)−N(2)	1.369(2)	N(1)−C(3)−N(2)	111.49(13)
C(3)−N(1)	1.3228(19)	C(3)−N(1)−C(1)	105.22(12)
C(3)−N(2)	1.338(2)	C(3)−N(1)−Fe(1)	124.28(10)
N(1)−Fe(1)	2.2038(11)	C(1)−N(1)−Fe(1)	130.26(10)
N(3)−O(1)	1.2514(11)	C(3)−N(2)−C(2)	107.64(14)

N(1)−C(1)−C(2)−N(2)	1.0(2)	C(2)−C(1)−N(1)−Fe(1)	−174.77(12)
N(2)−C(3)−N(1)−C(1)	−0.27(17)	N(1)−C(3)−N(2)−C(2)	0.88(19)
N(2)−C(3)−N(1)−Fe(1)	174.48(10)	C(1)−C(2)−N(2)−C(3)	−1.1(2)
C(2)−C(1)−N(1)−C(3)	−0.46(19)		

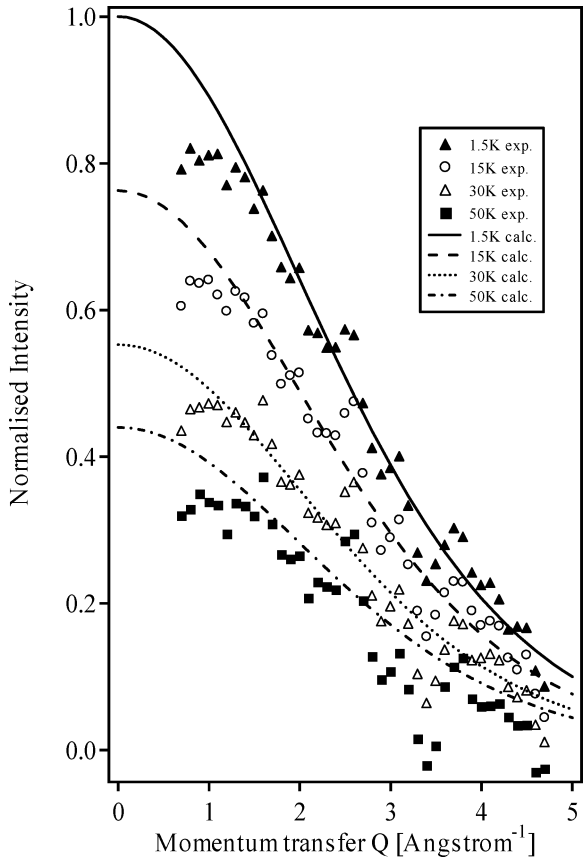

Figure 3. Plots of the intensities of transition *I* at various temperatures, as a function of increasing momentum transfer, *Q*.

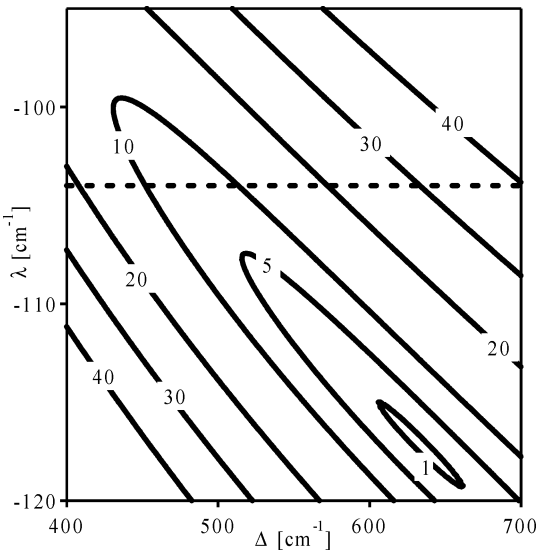

Figure 4. Contour plot of χ^2 as a function of the spin−orbit coupling constant λ and the trigonal field parameter Δ. The free ion value of λ is indicated by the dashed line.

prime labels) at elevated temperatures. The experimental energies and intensities are presented in Table 3. These results agree with previous measurements carried out on the time-of-flight-spectrometer FOCUS (see Supporting Information Figure S1). The magnetic peaks are assigned to transitions within the states of the $^5T_{2g}$ (O_h) ground term and are depicted in the inset of Figure 2. The symmetry labels, a and e, denote the degeneracy of the energy levels between which the transitions occur.

Transitions between the low-energy excitations of high-spin Fe(II) complexes are commonly reported within the framework of an $S = 2$ spin-Hamiltonian.[8] In the present study, the energy of the first excited state immediately suggests a value of $\sim$20 cm^{-1} for the axial spin-Hamiltonian parameter, *D*. The energy of the next level and the magnetic response of the system suggest that higher order terms would be needed to model the data with the conventional $S = 2$ spin-Hamiltonian. The zero-field splitting is very large, as the magnitude of the splitting of the $^5T_{2g}$ (O_h) ground term by the diagonal trigonal field is comparable to that by spin−orbit coupling. In this instance, it is more conducive to model the INS data directly from the ligand field wave functions. The INS spectra were interpreted using the Hamiltonian

$$\hat{H} = Dq\frac{-28\sqrt{\pi}}{3}\left(Y_4^{\,0} + \sqrt{\frac{10}{7}}(Y_4^{\,3} - Y_4^{\,-3})\right) + \Delta\frac{-14\sqrt{\pi}}{3\sqrt{5}}Y_2^{\,0} + \lambda\hat{L}\cdot\hat{S} \quad (1)$$

acting in the weak-field ^5D basis, where $Y_L^{m_l}$ denotes a normalized spherical harmonic function. The off-diagonal trigonal-field matrix elements between the cubic ^5E_g and $^5T_{2g}$ terms were ignored; Δ is then the diagonal trigonal field splitting of the $^5T_{2g}$ ground term and is positive when the nondegenerate orbital component is lower lying. The parameter 10Dq, describing the cubic ligand field, was fixed at 12 000 cm^{-1} as deduced from elementary single-crystal optical absorption measurements. The parameters λ and Δ were estimated from the experimentally determined energies by numerical diagonalization of the matrix representation of eq 1 and minimizing the function

$$\chi^2 = \sum_{j=1}^{2}\left(\frac{\Delta E_{\mathrm{calc},j} - \Delta E_{\mathrm{exp},j}}{\sigma_{\mathrm{exp},j}}\right)^2 \quad (2)$$

Table 3. Experimental and Theoretical Energies and Relative Intensities of the INS Transitions

			normalized intensities[a]							
	energies (cm^{-1})		1.5 K		15 K		30 K		50 K	
label	expt	calcd	expt	calcd	expt	calcd	expt	calcd	expt	calcd
I	19.4(2)	17.98	1.00	1.00	0.76(1)	0.74	0.56(1)	0.54	0.44(2)	0.43
II	75.7(6)	76.09			0.06(1)	0.05	0.13(1)	0.14	0.14(1)	0.16
I′	−19.1(6)	−17.98			0.06(1)	0.13	0.15(1)	0.23	0.18(1)	0.26

[a] The experimental intensities were scaled against transition I at 1.5 K.

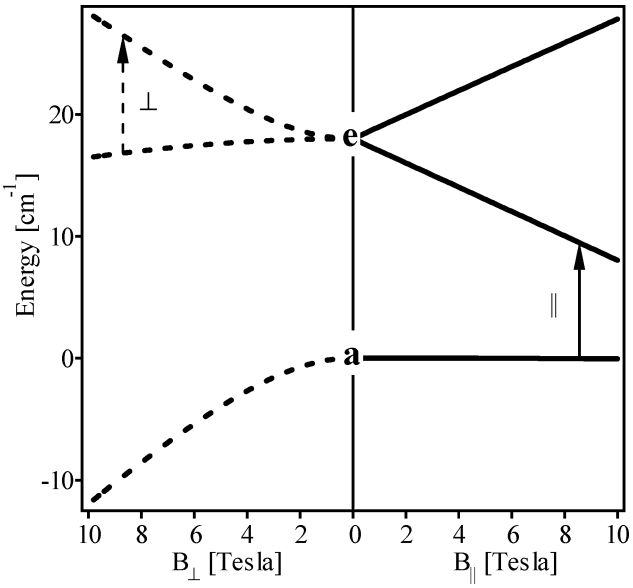

Figure 5. Plot of the calculated energies of the lower three energy levels as a function of field directed parallel and normal to the 3-fold axis. The energies were calculated using the best-fit parameters obtained from INS, with an orbital reduction factor $k = 1$. Arrows depict the observed EPR transitions.

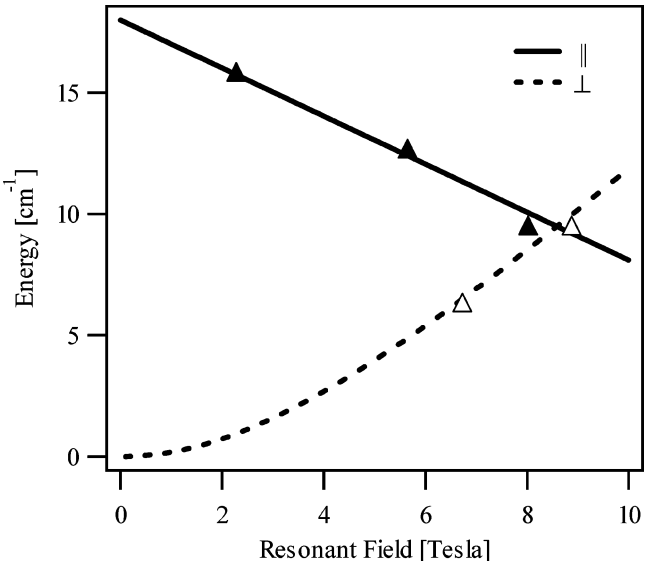

Figure 6. Plot of the transition energies versus resonant fields. The dashed and bold lines depict the calculated energies of the transitions || and ⊥ as a function of field. The experimental resonant field positions of the || and ⊥ transitions at specific frequencies are represented by open and full triangles, respectively.

where $\Delta E_{\mathrm{exp},j}$ and $\Delta E_{\mathrm{calc},j}$ are the jth experimental and calculated transition energies respectively, with $\sigma_{\mathrm{exp},j}$ the associated experimental error. The two energy differences correspond to those depicted in the inset of Figure 2. In Figure 4 a contour plot of χ^2 as a function of λ and Δ is shown. It is seen that a good fit ($\chi^2 \leq 1$) can be obtained only for a limited range of values of Δ and λ. Whilst a very good χ^2 is obtained for $\Delta = 632$ and $\lambda = -117$ cm^{-1}, the latter is larger in magnitude than the free ion value and consequently not physical. Applying the additional condition that $\lambda \geq -104$ cm^{-1} is applied, the free ion value, the energies are best modeled with $\lambda = -104$ and $\Delta = 485$ cm^{-1}.

The intensity, I_{INS}, of a magnetic transition between states with eigenvalues E_{i} and E_{f}, and eigenvectors, ψ_i and ψ_f, is proportional to[16]

$$I_{\mathrm{INS}} \propto F^2(Q)\rho_{\mathrm{i}}\frac{1}{3}\begin{Bmatrix}\langle\psi_i|k\hat{L}_z + g_e\hat{S}_z|\psi_f\rangle\langle\psi_f|k\hat{L}_z + g_e\hat{S}_z|\psi_i\rangle \\ + \langle\psi_i|k\hat{L}_x + g_e\hat{S}_x|\psi_f\rangle\langle\psi_f|k\hat{L}_x + g_e\hat{S}_x|\psi_i\rangle \\ + \langle\psi_i|k\hat{L}_y + g_e\hat{S}_y|\psi_f\rangle\langle\psi_f|k\hat{L}_y + g_e\hat{S}_y|\psi_i\rangle\end{Bmatrix} \quad (3)$$

where $F(Q)$ is the magnetic form factor, ρ_{i} is the Boltzmann factor of the initial state, k is the orbital reduction factor, and g_e is the free electron g value. The relative intensities were calculated at $Q = 0$ Å^{-1}, where $F(Q)$ is equal to unity, using the eigenvalues and eigenvectors resulting from the numerical diagonalization of eq 1, with $10Dq$, Δ, and λ set to 12 000, 485, and −104 cm^{-1}, respectively, and $k = 1$. The calculated intensities presented in Table 3 are seen to be in good agreement with the experimental values.

From Table 3 it is seen that the calculated energy of the first excited state is a little lower than the experimental value. This discrepancy is attributable to the limited electronic basis. Further calculations, incorporating all the states arising from the d^6 electronic configuration, were performed using the program LIGFIELD,[28] within the framework of the AOM. The calculated INS transition energies were not very sensitive to the values of the Racah parameters B and C, and these were set to 720 and 3100 cm^{-1}, respectively (~80% of the free ion values[29]). Using the crystal structure geometry as input, an exact reproduction of the experimental energies could be obtained with the parameters $\zeta = 394$ ($\zeta = -4\lambda$-(^{5}D)), $e_\sigma = 3953$, $e_{\pi,||} = 207$, and $e_{\pi,\perp} = 0$ cm^{-1}, where $e_{\pi,||}$ and $e_{\pi,\perp}$ model the Fe(II)−imidazole π-bonding normal to and in the plane of the imidazole ring, respectively.[30] These values are similar in magnitude to those determined previ-

(28) Bendix, J. *LIGFIELD Version 0.92*; Department of Chemistry, H. C. Ørsted Institutt, University of Copenhagen: Copenhagen, Denmark.
(29) Bendix, J.; Brorson, M.; Schaeffer, C. E. *Inorg. Chem.* **1993**, *32*, 2838−2849.
(30) If the treatment is confined to the $^5T_{2g}$ (O_h) ground term, the quantities $e_{\pi,||} - e_{\pi,\perp}$, Δ, and φ are related through the equation $\Delta = 3(e_{\pi,||} - e_{\pi,\perp})\sin(2\varphi)$,[23] from which a value of $e_{\pi,||} - e_{\pi,\perp} = 233$ cm^{-1} is obtained.

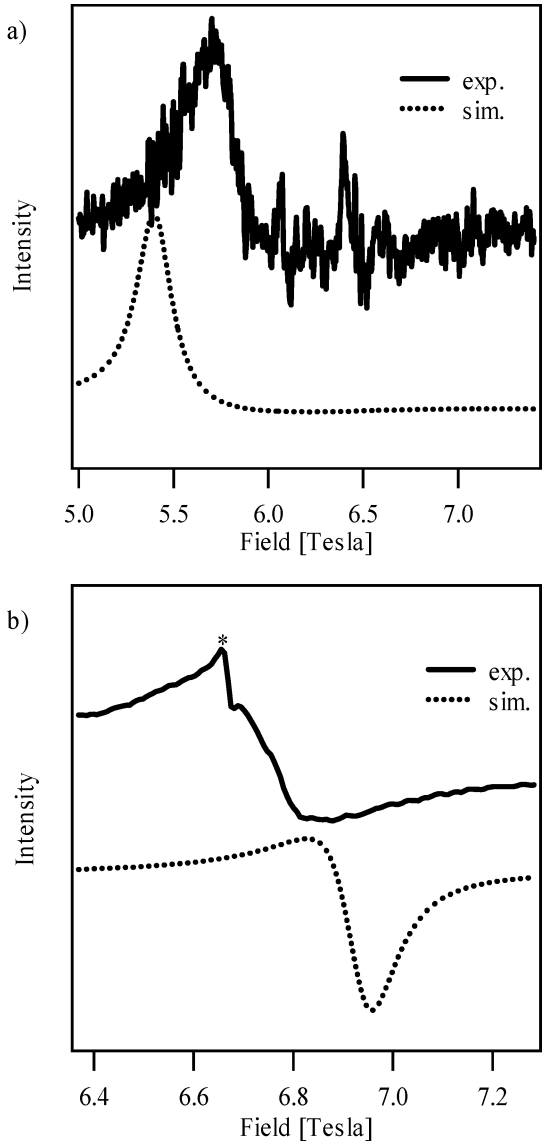

Figure 7. Plots of HF-EPR spectra of a powdered sample of $Fe(Im)_6(NO_3)_2$, obtained using excitation frequencies of (a) 379.9828 GHz (5 K) and (b) 190.005 GHz (25 K). Simulated EPR spectra are depicted by broken lines.

ously for the Fe(II)−pyridine interaction, $e_\sigma = 3700$, $e_{\pi,\parallel} = 100$, and $e_{\pi,\perp} = 0$ cm^{-1}, in the heteroleptic $Fe(py)_4(NCS)_2$ complex, where the Fe−N bond lengths are 2.241(4) and 2.268(4) Å compared to 2.204(1) Å in the present case.[5,31] The AOM parameters provide a reasonable first description of the Fe(II)−imidazole bonding interaction. However, in order to provide accurate estimates of the AOM parameters, the spectroscopic determination of higher lying states is required.

3.3. High-Field EPR. The HF-EPR data were modeled in the ^{5}D electronic basis using the Hamiltonian given in eq 1, extended to include the magnetic moment operator. In Figure 5 are presented plots of the calculated energies of the lowest three energy levels of the ^{5}D manifold, as a function of a magnetic field applied parallel and normal to the 3-fold axis of the molecule. The two observed EPR transitions are indicated by arrows and labeled || and ⊥. The energies were calculated by numerical diagonalization of the matrix representation of the Hamiltonian, using the best-fit parameters obtained from INS and an orbital reduction factor $k = 1$. The ⊥ transition is particularly weak, owing to the large zero-field splitting. Figure 6 shows plots of the calculated energies of transitions || and ⊥ as functions of the magnetic field. Superimposed on these plots are the experimental resonant field positions for these transitions at specific excitation frequencies, determined by fitting single and first derivative Lorentzian functions to the experimental data.

In Figure 7 are shown example powder EPR spectra obtained at 380 and 190 GHz, together with simulations. The observed transitions correspond to the || and ⊥ transitions, respectively. A narrow resonance, indicated by an asterisk, is observed superimposed upon the broad resonance of the $[Fe(Im_6)]^{2+}$ complex. This occurs in the $g = 2$ region of the spectrum and is due to a paramagnetic impurity. The simulations were produced with the EPR simulation software of Høgni Weihe,[32] using the Hamiltonian matrices constructed in the ^{5}D basis. No attempt is made here to optimize the parameters determined from the INS measurements. Nevertheless, the calculated resonant field positions and band shapes of the simulated spectra agree well with experiment. It was found that reasonable agreement with both the INS and EPR data could be obtained with $\lambda = -104$ cm^{-1} and Δ in the range 455 cm^{-1} < Δ < 510 cm^{-1}. Poor agreement with the EPR data was obtained using the parameters $\lambda = -117$ and $\Delta = 632$ cm^{-1}, corresponding to the minimum χ^2 of the fit to the INS data.

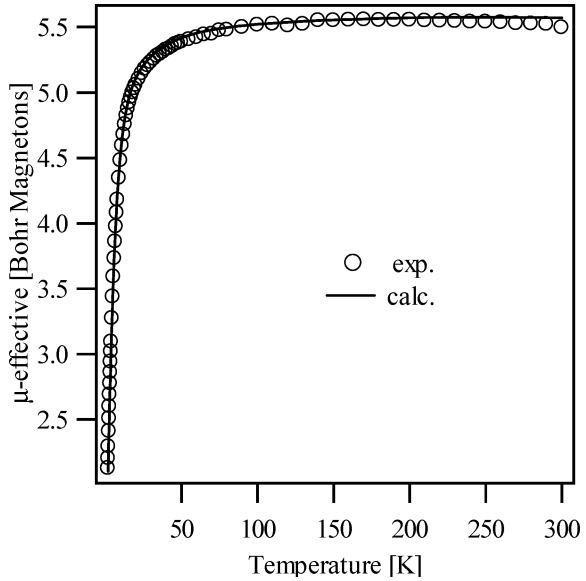

Figure 8. Plot of experimental and calculated μ_{eff} versus temperature for a powdered sample of $Fe(Im)_6(NO_3)_2$.

3.4. Magnetic Data. In Figure 8 is presented a plot of μ_{eff} versus temperature for a powdered sample of hydrogenous $Fe(Im)_6(NO_3)_2$. The experimental data points are shown as open circles. The solid line depicts the theoretical curve calculated from the ligand field Hamiltonian, con-

(31) Søtofte, I.; Rasmussen, S. E. *Acta Chem. Scand.* **1967**, *21*, 2028.

(32) Weihe, H., *sim Version 2001.6*; Department of Chemistry, H. C. Ørsted Institutt, University of Copenhagen: Copenhagen, Denmark, 2001.

structed in the ^{5}D basis and including the Zeeman interaction, using the best-fit parameters obtained from INS and an orbital reduction factor $k = 1$. The first derivatives of the energies with respect to the magnetic field were calculated using the Hellmann−Feynmann theorem. Again, whilst no attempt was made to optimize the ligand field parameters, the agreement between theory and experiment is striking.

4. Summary

INS data have been presented that enable a very precise definition of the low-energy electronic structure of the [Fe(Im)$_6$]$^{2+}$ cation. The energies and intensities of the magnetic transitions can be modeled quite satisfactorily by employing a ligand field Hamiltonian operating within the ^{5}D manifold. An excellent reproduction of HFMF EPR and susceptibility data is obtained using the wave functions and energies determined from the analysis of the INS data, giving further confidence to the model. The data permit the first estimates of the AOM bonding parameters, which should also be applicable to lower symmetry Fe(II)−imidazole complexes, where the mode of coordination is close to planar.

Acknowledgment. This work was funded by the Swiss National Science Foundation. We thank Stefan Janssen and Fanni Juranyi from the Laboratory for Neutron Scattering at PSI in Villigen, Switzerland, for their help in obtaining the INS data included as Supporting Information.

Supporting Information Available: X-ray crystal crystallographic files, in CIF format, listings of positional and thermal parameters for Fe($C_3H_4N_2$)$_6$(NO_3)$_2$, and figures showing INS spectra of a crystalline powder sample of Fe(Im)$_6$(NO_3)$_2$, obtained at 3.3 and 4.5 Å and at various temperatures on the time-of-flight spectrometer FOCUS. This material is available free of charge via the Internet at http://pubs.acs.org.

IC034110T